Simultaneous measurement of doping concentration and carrier lifetime in silicon using terahertz time-domain transmission

M. Lenz,[1] C. Matheisen,[2] M. Nagel,[2] and J. Knoch[1]
[1]*Institute of Semiconductor Electronics, RWTH Aachen University, Aachen 52074, Germany*
[2]*Protemics GmbH, Otto-Blumenthalstraße 25, 52074 Aachen, Germany*

(Received 2 December 2016; accepted 31 January 2017; published online 13 February 2017)

In this work, we present a measurement approach enabling the simultaneous determination of sheet resistance and carrier lifetime in semiconductor samples. It is based on a classic Terahertz (THz) time-domain transmission spectroscopy scheme extended by quasi-steady state optical excitation. The carrier lifetime is determined by contactless THz probing of the increase in sheet conductance associated with quasi-steady-state excitation. Combining a successive etch-back of the surface with repeated THz measurements yields a depth profile of the doping concentration and the carrier lifetime, which is important for the optimization of the emitter of solar cells, for instance. The viability of our approach is demonstrated by investigating a phosphorous doped emitter of a silicon solar cell with the THz approach and comparing the results with electrochemical capacitance voltage measurements. *Published by AIP Publishing*. [http://dx.doi.org/10.1063/1.4976314]

Appropriate doping is the key to realize various different functionalities of semiconductor devices such as diodes, transistors, and solar cells. Especially in photovoltaics, the impact of the doping profile of the emitter on the resulting carrier recombination is crucial. Every doping gradient causes an electrical field, leading to an acceleration of the involved excess carriers into a certain direction.[1,2] In particular, surfaces in close proximity to a doping profile play a determining role.

Semiconductor surfaces often exhibit a large interface state density (in the range of $>10^{15}\,\mathrm{cm}^{-2}$ in silicon), leading to, e.g., Fermi level pinning.[3–6] Such a high interface state density leads to a corresponding surface recombination velocity (SRV) larger than 10^6 cm/s, which is close to the thermal limit of electrons in silicon. A front surface field (FSF) can suppress this high recombination velocity at the interface since the difference of the doping concentrations causes an electrical field that pushes the excess carriers back into the interior of the semiconductor.[7,8] The emitter doping profile of a solar cell can have a similar effect on the excess carriers: After the light induced generation process, the emitter p-n junction separates electrons and holes. An optimized emitter profile can exhibit the same effect as a FSF, i.e., pushing the minority carriers away from the highly recombination-active surface and thus screening or effectively passivating the surface. Hence, the analysis of the influence of a doping profile on the resulting effective carrier concentration is the essential key that enables device optimization in this regard. Therefore, a measurement approach, which is capable to determine dopant concentration and carrier lifetime simultaneously, is highly desirable.

Current measurement approaches are usually able to determine only one of these parameters. E.g., with photoluminescence, the direct recombination of optically generated carriers is measured.[9,10] Coil based contactless photoconductance measurements detect the recombination current caused by the decay of optically generated excess carriers.[11,12] This latter technique does not measure excess carriers directly, though. Hence, the determination of an entire doping profile cannot be achieved with this method. Furthermore, the use of a coil sensor limits the resolution of this method.[13]

Approaches based on thermography, like Carrier Density Imaging,[14] are based on the absorption of infrared radiation by free carriers:[15] Therefore, free carriers are optically generated within the sample and probed by heat radiation in a wavelength range below 5 μm. In relation to terahertz (THz)-radiation, this wavelength provides a very low absorption coefficient, resulting in a limited detection sensitivity. A differentiation of local doping concentrations that would enable a depth-dependent measurement of the doping profile can therefore be considered impossible.

The approach utilized in this work is based on THz radiation generated and detected by photoconductive emitter and detector devices. The THz radiation is transmitted through a silicon sample,[16,17] which is placed in the focal point of the THz-beam. The transmission is attenuated according to the density of free excess carriers within the silicon sample.[18] The corresponding opto-electronic measurement setup is illustrated in Fig. 1.

For the THz generation, a Ti:Sapphire-laser beam is focused onto the backside of a THz transmission emitter (TeraBlast, Protemics GmbH), and for the detection, a photoconductive antenna is used.[19] The amplitude of the THz pulse is attenuated by free excess carrier absorption[18] and reflection loss at the air/silicon interface. As can be described by the Kramers-Kronig relation, the pulse transmitted through the sample is also delayed in relation to the reference pulse transmitted through air. The amplitude attenuation of the THz pulse provides information about the amount of free carriers and the sheet resistance of a semiconductor material.[20]

In order to measure a full depth-dependent doping profile, the access of the THz-transmission to the sheet conductivity can be utilized. By etching back the semiconductor surface, the amount of dopants contained in the etched back volume between two discrete depths d_i and d_{i-1} can be determined. The corresponding sheet resistance R_i in the depth d_i

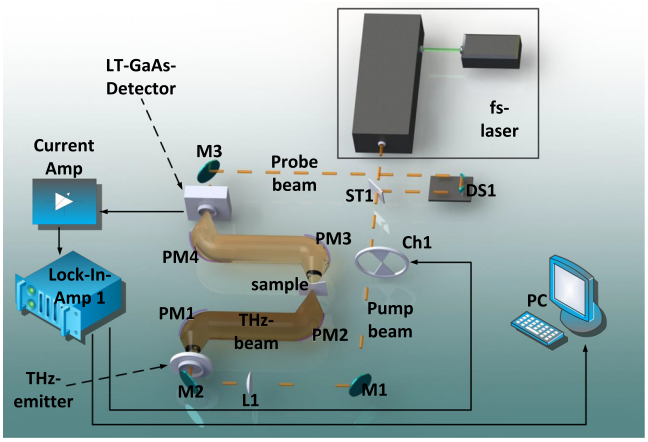

FIG. 1. Optical and electrical setup to sample a time transient of the THz-pulse transmission.

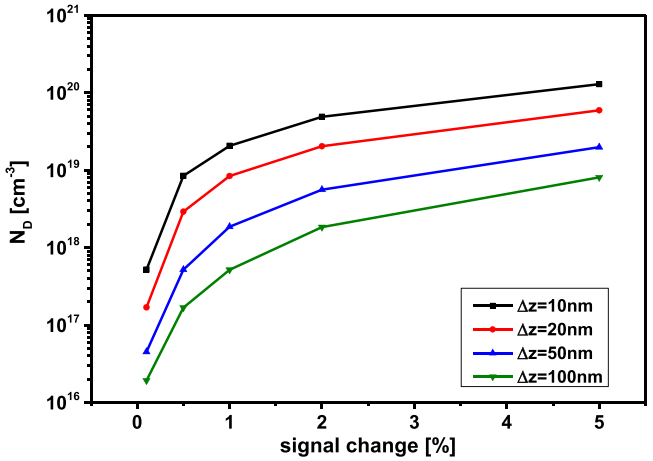

FIG. 2. Signal change of the transmitted THz-power and the corresponding measureable doping concentration for different depth resolutions Δz. For larger Δz, the corresponding signal changes get larger; thus, less concentrations can be measured with the same SNR.

can be measured by relating the initial sheet resistance R_0 (without etching) to its corresponding THz transmission signal S_0 and the transmission signal S_i

$$R_i = \frac{R_0}{S_0} S_i. \tag{1}$$

The conductivity of the profile to be measured is inversely proportional to the sheet resistance

$$\int_0^{z_I} \sigma(z)dz = \frac{1}{R_{Sh}}. \tag{2}$$

Hence, the conductivity of the etched back volume between the depth d_i and d_{i-1} can be calculated by

$$\Delta\sigma_i = \frac{1}{R_{Sh,i}} - \frac{1}{R_{Sh,i-1}}. \tag{3}$$

The resulting $\Delta\sigma_i$ values can be used for the computation of the desired doping concentration N_i in the depth di

$$N_i = \frac{\Delta\sigma_i}{\Delta z_i e \mu_i}. \tag{4}$$

It should be mentioned that the doping concentration N_i represents the mean concentration between the depth d_i and d_{i-1}. Furthermore, it is necessary to consider the influence of the doping concentration on the carrier mobility[21] given by

$$\mu_i = \mu_{\max} + \frac{\mu_{\max} - \mu_{\min}}{1 + \left(\frac{N_i}{N_r}\right)^{\alpha}}. \tag{5}$$

The main limiting factor of this approach is given by the noise limit, which determines the smallest discriminable signal variation ΔS_i between two adjacent depths to resolve a certain dopant concentration N_i. For that purpose, the doping concentration is calculated in dependency of the signal change for four different depth differences Δz between 10 nm (black curve in Fig. 2) and 100 nm (green curve in Fig. 2). It can be seen that for smaller Δz, a higher measurement accuracy is required. Correspondingly, for a given uncertainty level of 0.5%, a depth resolution down to 10 nm can be achieved for high doping concentrations $N_D > 10^{19}\,\mathrm{cm}^{-3}$, whereas for lower concentrations $N_D < 10^{17}\,\mathrm{cm}^{-3}$ Δz has to be larger than 100 nm.

The determination of the carrier lifetime requires a deviance from the equilibrium state. To this end, free excess carriers Δn_{eff} are generated by optical excitation and the corresponding difference of sheet resistance is measured by THz-pulse transmission. By using a red light excitation source, an absorption length of approximately $d_\alpha = 1\,\mu$m can be assumed. Together with the assumption of low level injection, Tinkham's formula[22] can be utilized to calculate the difference of the THz-transmission T between the illuminated S_{illu} and the non-illuminated state S_0

$$T = \frac{S_{illu}}{S_0} = \frac{1}{1 + \sigma_{sh}\dfrac{Z_0}{n_{THz}+1}}, \tag{6}$$

with $Z_0 = 377\,\Omega$ being the impedance of free-space and $n_{THz} = 3.39$ the refractive index of silicon in the THz range. Due to the small amount of excess carriers compared to the entire amount of dopants, n_{THz} can be assumed to be constant. With substituting σ_{sh}, the effective carrier lifetime can be expressed as the difference of the transmitted THz-pulse amplitudes S_0 and S_{illu}

$$\tau_{eff} = \frac{n_{THz}+1}{e\mu_n G d_\alpha Z_0}\left(\frac{S_0 - S_{illu}}{S_{illu}}\right) = C\frac{\Delta S}{S_{illu}}. \tag{7}$$

For silicon, we assume a constant carrier mobility of $\mu_n = 800\,\mathrm{cm}^2/\mathrm{V\,s}$. A more accurate determination of μ_n can also be obtained by the integration of Eq. (5). Including—as an example—a generation rate of $G \sim 10^{20}\,\mathrm{cm}^{-3}\,\mathrm{s}^{-1}$ and an absorption depth of 10^{-6} m for 610 nm (red) light illumination at 100 mW/cm^2, the constant C becomes $\sim 10^{-2}$ s.

The configuration of the measurement setup enabling the simultaneous measurement of sheet resistance and carrier lifetime is shown in Fig. 3. The basic setup (Fig. 1) is expanded by the components highlighted in red.

All measurements are differential and carried out at the THz-peak value; thus, neither the THz spectrum nor the THz

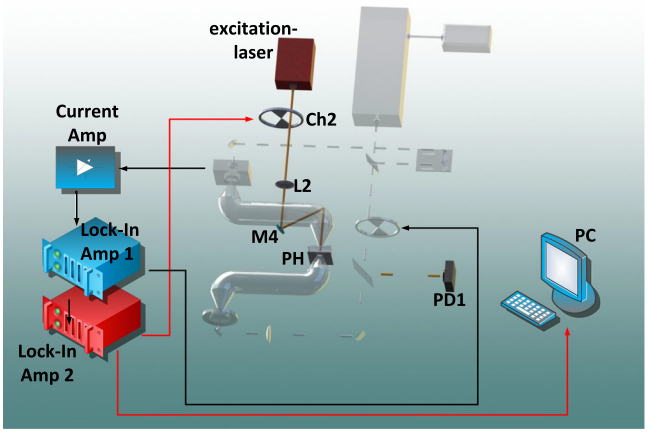

FIG. 3. Optical and electrical setup to measure the doping profile and carrier lifetime simultaneously. The highlighted components are integrated into the faded fundamental setup.

power has an influence on the recorded results and the determined values. A 2-mm-diameter pinhole (PH) is placed directly in front of the sample in order to enhance the lateral resolution. In order to achieve the necessary measurement accuracy, computed in Fig. 2, a photodiode is integrated into the pump-beam path. By continuously monitoring the optical power of the pump beam, fluctuations of the femtosecond laser are compensated. In the basic setup, typically time transients are measured; thus, this compensation of the power fluctuations is not necessary. For small deviations of the laser output power, a linear correction is assumed. Therefore, the averaged measurement value of the THz-transmission signal is calculated from

$$S = \sum_i S_i \frac{P_{fs,1}}{P_{fs,i}}. \tag{8}$$

The reading S_i is thus normalized with the monitored laser power in relation to the first reading. As depicted in Fig. 4, the measurement accuracy is approximately doubled with this method. To determine the performance of this correction method, a series of THz transmissions are recorded in dependency of the number of averages. The results are shown in Fig. 4. The blue symbols represent the measurement without correction and the red symbols display the corrected measurement. Further, the filled dots represent the raw readings and the open symbols the corresponding averaged values. The associated standard deviation is visualized by the bars. It is shown that an uncertainty level of 0.17% can be achieved by averaging over 200 readings. According to Fig. 2, a doping concentration of less than $10^{17}\,\mathrm{cm}^{-3}$ can be resolved for an etched-back depth of 50 nm, whereas for an etched depth of $\Delta z = 10$ nm, a concentration of less than $10^{18}\,\mathrm{cm}^{-3}$ can still be resolved.

In order to verify this measurement principle, a THz transmission measurement on a phosphorous diffused doping profile exhibiting a sheet resistance of 110 Ω/sq. is compared with an electrochemical capacitance-voltage (ECV)-measurement[23,24] as illustrated in Fig. 5(a). Both profiles are in reasonable good agreement. The much higher doping density and thus the corresponding higher measurement sensitivity (compare Fig. 2) enable a better matching with the ECV-measurement.

The sample excitation necessary for the carrier lifetime determination is implemented by a red (wavelength: 610 nm) continuous wave laser, integrated into the setup.[19] To suppress carrier diffusion effects, a sufficiently large excitation spot size of 19 mm^2 is used by embedding lens L2 (cf. Fig. 3) into the excitation beam path. With a maximum optical power of 50 mW, the illumination intensity can be increased up to 260 $\mathrm{mW/cm}^2$. To directly measure ΔS (cf. Eq. (7)), a second lock-in amplifier is used and the sample is periodically illuminated by chopper wheel 2 (Ch2) with a frequency of 22.3 Hz.

The verification of the carrier lifetime measurement method is carried out on a front surface field, induced by a $POCl_3$ process on a n-type silicon wafer. The resulting doping profile was measured with ECV and is shown in Fig. 5(b) (black curve). The surface concentration is $10^{19}\,\mathrm{cm}^{-3}$, and the depth of the doping diffusion can be extracted to approximately 100 nm. The depth dependent carrier lifetime profile measured with THz-pulse transmission is also shown in Fig. 5(b) (blue curve), confirming the strong dependency

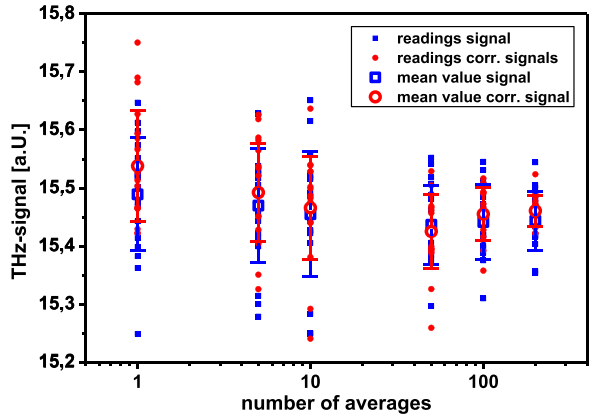

FIG. 4. Verification of the measurement uncertainty: THz-transmission in dependency on the number of averages. The rectangular symbols show the uncorrected readings, the circles depict the corrected values, the filled symbols represent single readings, and the open symbols are the corresponding mean values. The deviation can be decreased to 0.17% for 200 averages.

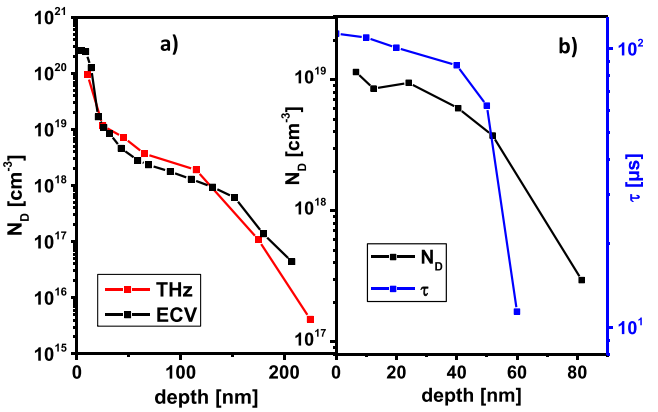

FIG. 5. (a) Comparison of a phosphorous doping profile measured with THz-transmission (red curve) and with ECV (black curve). (b) Depth dependent THz-carrier lifetime measurement of a front surface field in the logarithmic scale (blue curve) and the corresponding doping profile measured with ECV (black curve).

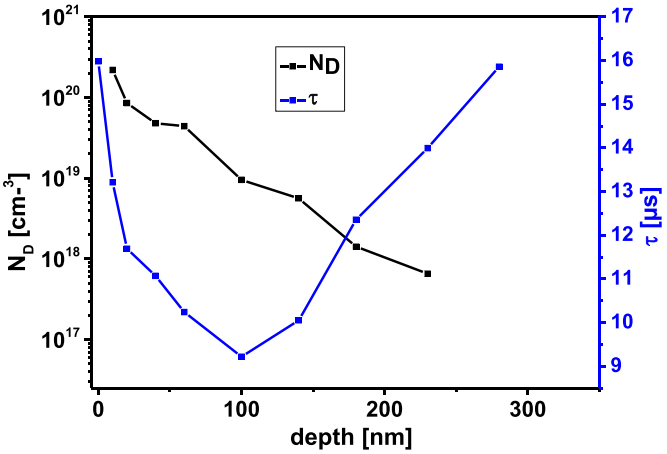

FIG. 6. Simultaneous measurement of the carrier lifetime (blue curve) and doping profile (black curve). The concentration gradient near the surface yields an effective increase of the carrier lifetime τ_{eff} down to a depth of approximately 100 nm.

to carrier concentration. Near the surface, the lifetime has a maximum value of $\tau_{eff} = 111\ \mu s$. With etching back the FSF τ_{eff} decreases rapidly. The strongest decline of the carrier lifetime can be observed between a depth of 50 and 60 nm. The removal of dopants beneath $\sim 10^{18}\ cm^{-3}$ causes a significant performance drop of the electrical field passivation of the FSF. After completely removing the doping profile, the lifetime reaches its minimum value of $\tau_{eff} = 10\ \mu s$.

As described in the previous paragraphs, THz-pulse transmission allows a simultaneous measurement of the doping concentration N_D and the effective carrier lifetime τ_{eff}. Thus, a direct correlation between these two parameters can be obtained. In the case of a p-n-junction as in an emitter of a solar cell, the gradient of the doping concentration causes an electrical field that screens the recombination, thus effectively passivating the surface (comparable to the previously investigated FSF). This effect can be observed in Fig. 6, showing a simultaneous depth dependent determination of N_D (black curve) and τ_{eff} (blue curve).

For this measurement, a sample based on a 200 μm thick p-type silicon wafer exhibiting a conductivity of 3–5 Ω cm was prepared. The doping profile was diffused using a $POCl_3$-process, resulting in a sheet resistance of 110 Ω/sq. The strongest decline of N_D from $2 \times 10^{20}\ cm^{-3}$ to $5 \times 10^{19}\ cm^{-3}$ within a depth of 40–50 nm is located directly beneath the surface. This rapid decline provides a strong electrical field effect, which is reflected in the carrier lifetime curve. A drop of $\tau_{eff} = 16\ \mu s$ to 9 μs is observable, which corresponds to an improvement of 38% caused by the field effect. Below a depth of 100 nm, τ_{eff} increases again. In this case, the electrical field of the p-n-junction, and hence a pronounced carrier screening effect, is located closer to the surface. This correlation can be seen by the simultaneous measurement (cf. Fig. 6) and can be used to improve the design of minority carrier devices like solar cells.

In this work, we demonstrated a measurement technique for the simultaneous determination of sheet resistance and carrier lifetime values in semiconductors. In addition, the successive etching of the sample surface enables a full depth-dependent measurement of both parameters. The measurement facilitates a detailed investigation of the influence of doping profiles on the resulting carrier lifetime. The method was demonstrated at a phosphorous diffused doping profile, where a surface-near field effect caused by a strong doping gradient could be observed. The measurement technique can be employed to other semiconductor materials. In a next step, this measurement method will be adapted to THz near-field probing, enabling a lateral resolution down to approx. 50 μm.

[1]F. Granek, C. Reichel, M. Hermle, D. M. Huljić, O. Schultz, and S. W. Glunz, in *22nd European Photovoltaics Solar Energy Conference* (2007), p. 1454.
[2]J. G. Fossum and E. L. Burgess, Appl. Phys. Lett. **33**, 238 (1978).
[3]F. J. Himpsel, G. Hollinger, and R. A. Pollak, Phys. Rev. B **28**, 7014 (1983).
[4]T. Nishimura, K. Kita, and A. Torium, Appl. Phys. Lett. **91**, 123123 (2007).
[5]J. D. Dow, O. F. Sankey, and R. E. Allen, Appl. Surf. Sci. **22/23**, 937 (1985).
[6]J. Tersoff, Surf. Sci. **168**, 275 (1986).
[7]X. M. Dai and Y. H. Tang, Sol. Energy Mater. Sol. Cells **43**, 363–376 (1996).
[8]O. von Roos, J. Appl. Phys. **50**, 5371 (1979).
[9]J. A. Giesecke, M. C. Schubert, B. Michl, F. Schindler, and W. Warta, Sol. Energy Mater. Sol. Cells **95**, 1011 (2011).
[10]S. Herlufsen, K. Bothe, J. Schmidt, R. Brendel, and S. Siegmund, Sol. Energy Mater. Sol. Cells **106**, 42 (2012).
[11]R. A. Sinton and A. Cuevas, Appl. Phys. Lett. **69**, 2510 (1996).
[12]R. A. Sinton and A. Cuevas, in *25th IEEE Photovoltaic Specialists Conference (PVSC)* (1996), p. 457.
[13]M. Morozov, G. Rubinacci, A. Tamburrino, and S. Ventre, IEEE Trans. Magn. **42**(5), 1568 (2006).
[14]J. Isenberg, S. Riepe, S. W. Glunz, and W. Warta, in *29th IEEE Photovoltaic Specialists Conference (PVSC)* (2002), p. 266.
[15]D. K. Schroder, R. N. Thomas, and J. C. Swartz, IEEE J. Solid-State Circuits **13**, 180 (1978).
[16]J. Neu and M. Rahm, Opt. Express **23**, 12900 (2015).
[17]L. Fekete, P. Kuzel, H. Nemec, F. Kadlec, A. Dejneka, J. Stuchlík, and A. Fejfar, Phys. Rev. B **79**, 115306 (2009).
[18]M. V. Exter and D. Grischkowsky, Phys. Rev. B **41**, 12140 (1990).
[19]M. Lenz, A. Kianfar, S. Nordmann, S. Sawallich, M. Nagel, B. Berghoff, and J. Knoch, in 42th IEEE Photovoltaic Specialists Conference (PVSC) (2015).
[20]M. Nagel, A. Safiei, S. Sawallich, C. Matheisen, T. M. Pletzer, A. A. Mewe, N. van der Borg, I. Cesar, and H. Kurz, in *28th European Photovoltaics Solar Energy Conference and Exhibition* (2013), p. 856.
[21]D. M. Caughey and R. E. Thomas, Proc. IEEE **55**, 2192 (1967).
[22]M. Tinkham, Phys. Rev. **104**, 845 (1956).
[23]P. Blood, Semicond. Sci. Technol. **1**, 7 (1986).
[24]E. Peiner and A. Schlachetzki, J. Electrochem. Soc. **142**, 576 (1995).